ELSEVIER

Spectrochimica Acta Part A 57 (2001) 2061–2069

SPECTROCHIMICA ACTA PART A

www.elsevier.com/locate/saa

Mapping the chemistry in nanostructured materials by energy-filtering transmission electron microscopy (EFTEM)☆

Ferdinand Hofer [a,*], Peter Warbichler [a], Hermann Kronberger [b], Josef Zweck [c]

[a] *Forschungsinstitut für Elektronenmikroskopie, Technische Universität Graz und Zentrum für Elektronenmikroskopie Graz, Steyrergasse 17, A-8010 Graz, Austria*

[b] *Institut für Technische Elektrochemie und Festkörperchemie, Technische Universität Wien, Wien, Austria*

[c] *Institut für Experimentelle u, Angewandte Physik, Universität Regensburg, D-93040, Regensburg, Germany*

Received 15 November 2000; accepted 15 January 2001

Abstract

Energy-filtered transmission electron microscopy (EFTEM) can be used to acquire elemental distribution maps at high lateral resolution within short acquisition times, which makes it quite efficient for a detailed characterization of nanostructures, as illustrated with examples concerning a nanostructured substituted La-based cermet compound and a nanoscale multilayer. In the first example, we show how phases in a rapidly cooled substituted $LaNi_5$ can be visualized by recording jump ratio images. Secondly, EFTEM was capable of imaging individual nanoscale layers in a magnetic multilayer consisting of 2 nm terbium and 3 nm iron.

Keywords: Energy-filtering transmission electron microscopy; Electron energy-loss spectrometry; Fe–Tb multilayer; La-based cermet

1. Introduction

Energy-filtering transmission electron microscopes (EFTEMs) have become important new tools in analytical electron microscopy both in materials and biological sciences [1–5]. In contrast to the traditional energy-dispersive X-ray and electron energy-loss spectroscopy methods, which are based on focusing a small probe on the specimen area of interest, EFTEM makes it possible to acquire images showing the two-dimensional intensity distribution of the electrons, which have lost a certain amount of energy due to inelastic scattering in the specimen. These electrons form the electron energy-loss spectrum (EELS) of the forward transmitted beam constituting a wide spectral band spectroscopy giving access to the electron excitation spectrum of the target from typically the eV to the keV domain [6]. EFTEM provides all EELS information in a spatially resolved character which makes it particularly well suited to the exploration of the local chemical and also electronic properties of nanostructures and nanostructured materials with dimensions in the nanometer range [7].

☆ Dedicated to Professor Harald P. Fritzer on the occasion of his retirement.

* Corresponding author. Tel.: +43-316-8738820; fax: +43-316-811596.

E-mail address: ferdinand.hofer@felmi-zfe.at (F. Hofer).

1386-1425/01/$ - see front matter
PII: S1386-1425(01)00488-7

The aim of the present paper is to highlight the possibilities of the technique and to emphasize the variety of materials science problems which can be solved by EFTEM and EELS.

1.1. Instrumentation: the present status

Energy-filtering microscopy has become well established only during the last few years, largely because of the availability of high performance commercial filters (Fig. 1). Fixed beam energy-filtering TEMs first form an unfiltered image (or diffraction pattern), then transform the image into an electron energy-loss spectrum, select a specific part of the spectrum, and finally transform the spectrum back into an energy-filtered image (or diffraction pattern).

Two types of energy-filters have become widespread: Firstly, post-column filters which bend the electron beam by 90° are located after the main column of the TEM [8,9] and alternatively, in-column energy-filters of omega like geometry consisting of four magnetic prisms which are located inside the projector lens system of the TEM [10,11].

Both types are operated in a very similar manner. In order to form an energy-filtered image, where the contrast is caused by energy-loss electrons from an energy range selected with an energy-selecting slit (positioned in the energy-dispersive plane), the EELS-spectrum is shifted relative to the energy-selecting slit. The width of the slit can be varied from 0 to 60 eV. After the zero-loss peak of the EELS-spectrum is adjusted on the optical axis, the energy-shift is made by increasing the acceleration voltage of the microscope by $+\Delta E$ to keep the energy-loss electrons of interest (ΔE) on the optical axis. An unfiltered image can be simply obtained by withdrawing the energy-selecting slit. Either an image or diffraction pattern can be filtered by changing the strength of the intermediate lens preceding the spectrometer system. Because the images are formed in parallel, elemental maps can be acquired in seconds to tens of seconds rather than tens of minutes to hours as required by the pixel-by-pixel scanning TEM approach. In addition to energy-filtered images it is also possible to acquire EELS-spectra in parallel. Images and spectra are mostly recorded on charge coupled devices (CCD) thus offering the advantage of a high detective quantum efficiency (DQE) as well as great dynamic range and good linearity [12]. Images and spectra recorded with CCD arrays have to be corrected for dark current, gain variations and sometimes also for the blurring which is caused by the point-spread function of the scintillator [13].

1.2. About the nanostructures to be investigated

Depending on the performance of the instrument, a large variety of problems and specimens with dimensions in the nanometer range can now be investigated. These include all types of objects and structures exhibiting small sizes in 1, 2 or 3 dimensions, such as small particles, interfaces and multilayers oriented so that the direction with the strong gradients in composition and/or topography lie perpendicular to the direction of the electron beam [14]. The most simple case deals with nanoparticles or clusters deposited on a thin supporting film (Fig. 2). A more complicated situation arises in case of interfaces or multilayers, because the features have to be aligned relative to the beam direction (Fig. 2).

Finally all types of composite material made of a combination or juxtaposition of nanometer sized components can also be investigated, although it becomes more difficult to avoid overlapping information along the direction of propagation of the electron beam (Fig. 2). If the size of the feature under investigation is smaller than the specimen thickness, problems may arise. This is due to the fact that the TEM produces a 2-dimensional projected image of a 3-dimensional specimen [15].

1.3. The information content of EELS and EFTEM

Over the energy range covered by EELS spectroscopy under high energy electron impact, one deals with the excitation of electrons in a solid. In the low energy-loss region ranging from 0 to about 50 eV, the quasi-free gas of valence or conduction electrons reacts as a whole (plasmons)

or as a population of individual electron-hole pairs (intra- or interband transitions), which is governed by the joint density of electronic states. In the high energy-loss region (commonly from about 50 to 2000 eV), inner shell electrons in individual atoms are excited. Therefore, in this

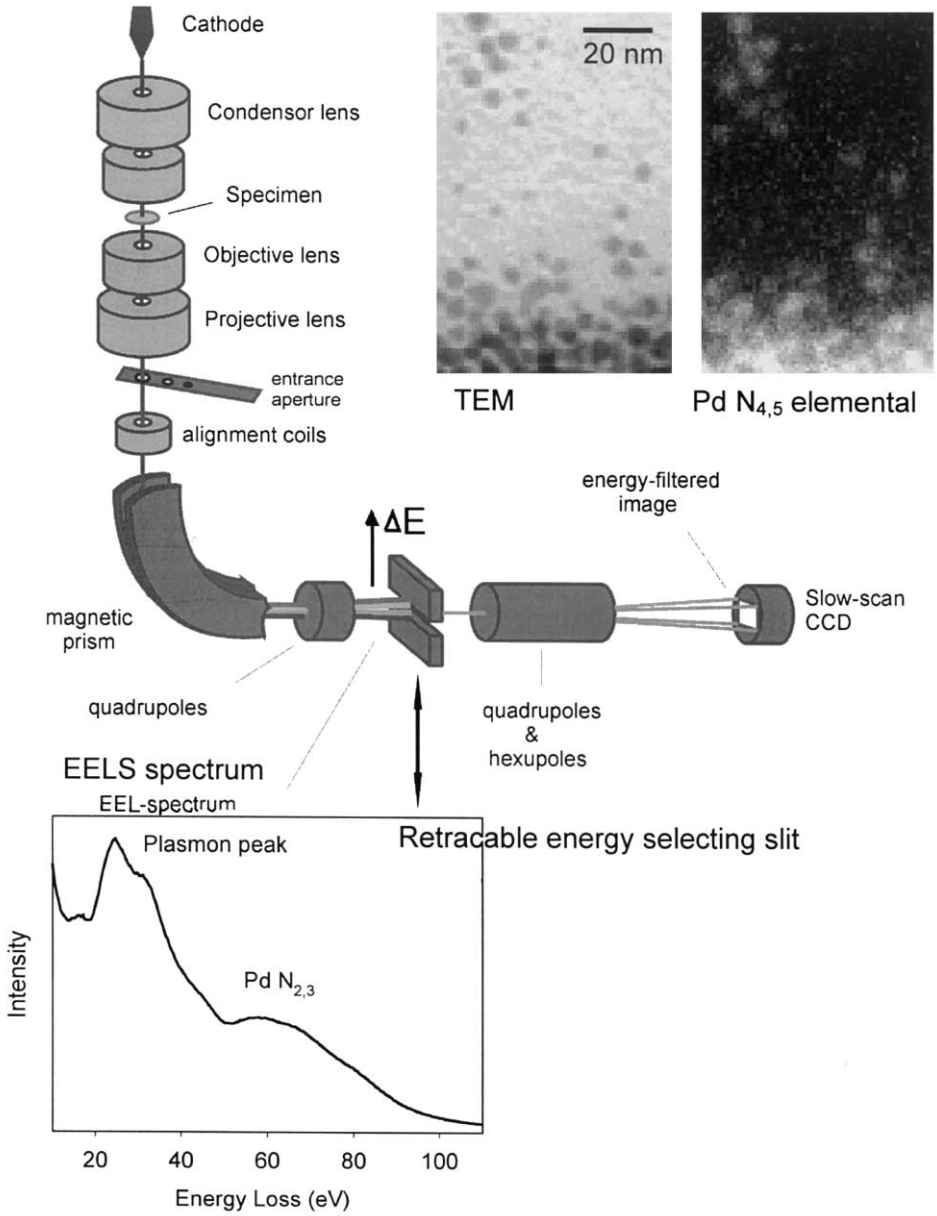

Fig. 1. Schematic illustration of the main components of an energy-filtering transmission electron microscope with an example of a TEM image of Pd clusters, the EELS spectrum recorded from the same specimen area and of a Pd elemental map calculated from energy-filtered images around the $PdN_{4,5}$ ionization edge.

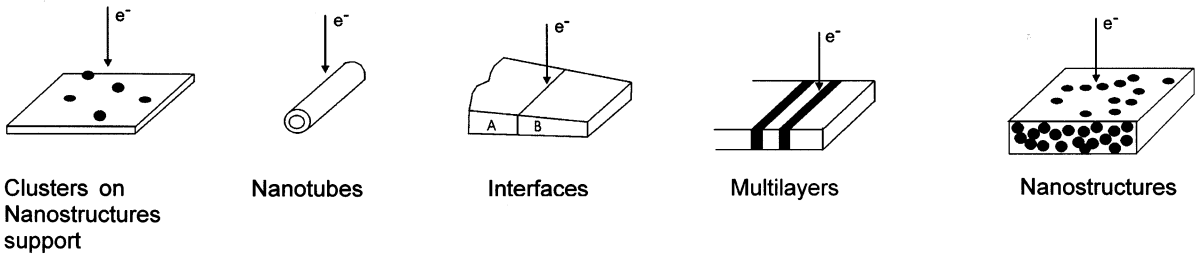

Fig. 2. Beam–specimen geometry of typical situations where the high spatial resolution of energy filtering TEM can be used to study clusters, nanotubes, interfaces, multilayers and nanostructured materials.

region EELS investigates the atomic character in a solid, including the elemental analysis carried by the specificity of the initial level of the transition, as well as the electronic information contained in the fine structures of the ionization edges [5]. Although all structures contained in electron energy-loss spectra are not yet fully understood, most features can nowadays be properly interpreted due to the substantial progress in the last 10 years. These new possibilities have recently been exploited for characterizing many types of specimens of variable geometry and composition [16].

Equipping a TEM with an energy-filter offers extraordinary advantages for the characterization of both materials science and biological samples [7]. Being able to select any spectral feature from an EELS-spectrum opens up a variety of new imaging techniques: Zero loss imaging improves contrast and resolution of TEM images and electron diffraction patterns by removing inelastic scattering; energy-filtered TEM imaging for 'tuning' the contrast of heterogeneous specimens; relative thickness mapping to image a specimen's thickness in units of mean free path; chemical mapping that enables imaging the specimen's local electronic structure. However, the most obvious advantage of EFTEM imaging is to derive compositional information by making use of the element specific ionization edges in the form of elemental maps [7,17]. In the next section we demonstrate how the EFTEM compositional mapping can be used for characterizing nanostructures of strong potential interest.

2. Experimental

The EELS-spectra and the energy-filtered images presented in this work were recorded using a Gatan Imaging Filter (GIF) mounted on a Philips CM2O TEM/STEM operated at 200 kV with a LaB_6 cathode. All images and EFTEM elemental maps were recorded with the slow-scan CCD camera of the GIF. The spectra were acquired in TEM image mode using a probe half angle of 1.5 mrad and a collection half angle of 7.6 mrad; a spectrometer dispersion of 0.5 eV/channel was used. For elemental mapping the signal-to-noise ratio (SNR) had to be optimized according to previously published recommendations [18,19]. We used the largest condenser aperture on the microscope (200 μm) and, because we are mainly measuring lower energy-losses, the 40 μm objective aperture (acceptance half angle of 7.6 mrad) was chosen. Other important parameters are the width and the position of the post edge window. Adjusting the window width and position to the respective edge type and energy-loss, we achieved an optimal SNR using window widths of 5 eV which is also advantageous for obtaining elemental maps at high spatial resolution.

All energy-filtered images were recorded using a binning of 2×2 giving 512×512 pixel images, for reasons of sensitivity. Since the focus for an energy-filtered image differs from that of the elastic image, we adjusted the focus for energy-filtered images at an energy-loss of about 60 eV. Since the investigated specimens were sensitive to radiation damage, the emission current was set to a current density of lower than 2 A/cm^2 and short acquisi-

tion times of about 2–5 s were used. Images and spectra were processed with Gatan's Digital Micrograph software package. All images and spectra were corrected for dark current and gain variation, however, they were not corrected for the blurring caused by the point spread function of the detector. Drift between successive images was corrected using a cross-correlation algorithm.

For elemental mapping it is necessary to remove the background contribution to the image intensity. To obtain elemental maps we used the three window technique [20]: Two energy-filtered background images in front of the edge and one energy-filtered image at the ionization edge of the element of interest have been recorded. Then an extrapolated background image below the edge is calculated by fitting the pre-edge images with a power-law model and the extrapolated background is subtracted from the ionization edge image thus giving the net elemental map (Fig. 3). In order to increase the signal-to-noise ratio of the elemental maps, we have additionally calculated jump ratio images by dividing the post-edge image by a pre-edge image [16]. In this work we mainly present jump ratio images which give for the examples presented in this paper the same information content as the elemental maps (calculated with the three window technique). However, it should be noted that the jump ratio images cannot be used for quantification and sometimes they

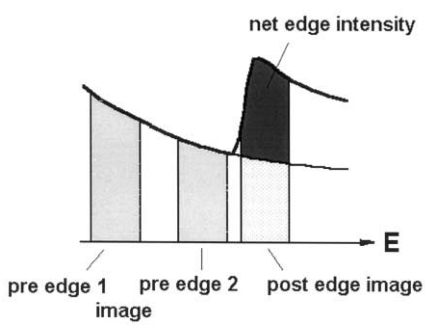

Fig. 3. The principle of background correction beyond an ionization edge is shown; the background is to be removed to obtain the net elemental map. At least two pre-edge images have to be acquired to calculate a background image which has to be subtracted from a post-edge image (for each pixel of the image). A jump ratio image can be calculated by dividing the post-edge image and a pre-edge image.

are susceptible to background slope changes due to specimen thickness variations. Therefore, it is necessary that in every case elemental maps are acquired using the three window method and jump ratio images can then be calculated afterwards. Further image processing of the elemental maps is often required, because, in addition to elemental contrast, contrast can also arise from mass thickness and diffraction effects. Especially the diffraction effects occurring in crystalline materials cause problems for reliable elemental mapping. Recently, it could be shown that these diffraction effects can be almost completely eliminated, if the energy-filtered images are acquired under rocking beam illumination [21].

All specimens were prepared following the standard TEM preparation techniques with final low angle ion-milling.

3. Results

3.1. Nanostructured La-based cermet

Structure–property correlation plays an important and increasing role in the design of advanced nanostructured materials which may consist of building blocks that contain a few to a few thousand atoms. The resulting materials have characteristic dimensions in nanometers and the properties of these materials depend on the properties of the individual building blocks, as well as their collective behaviour when consolidated.

One possible route to prepare nanostructured materials is to decompose a thermodynamically unstable compound, eg via a spinodal decomposition mechanism which leads to a modulated structure often with periodicities on the nanometer length scale.

In the present example we characterized rapidly cooled $LaNi_5$ which was substituted with Ce, Mn and Co. The material has the $CaCu_5$ structure and was prepared by heating La, Ni, Co, Ce and Mn followed by rapid cooling in air [22]. Since the intermetallic compounds of the $LaNi_5$ type form reversible hydrides either by solid–gas or by electrochemical reaction, these materials are of potential interest for hydrogen storage.

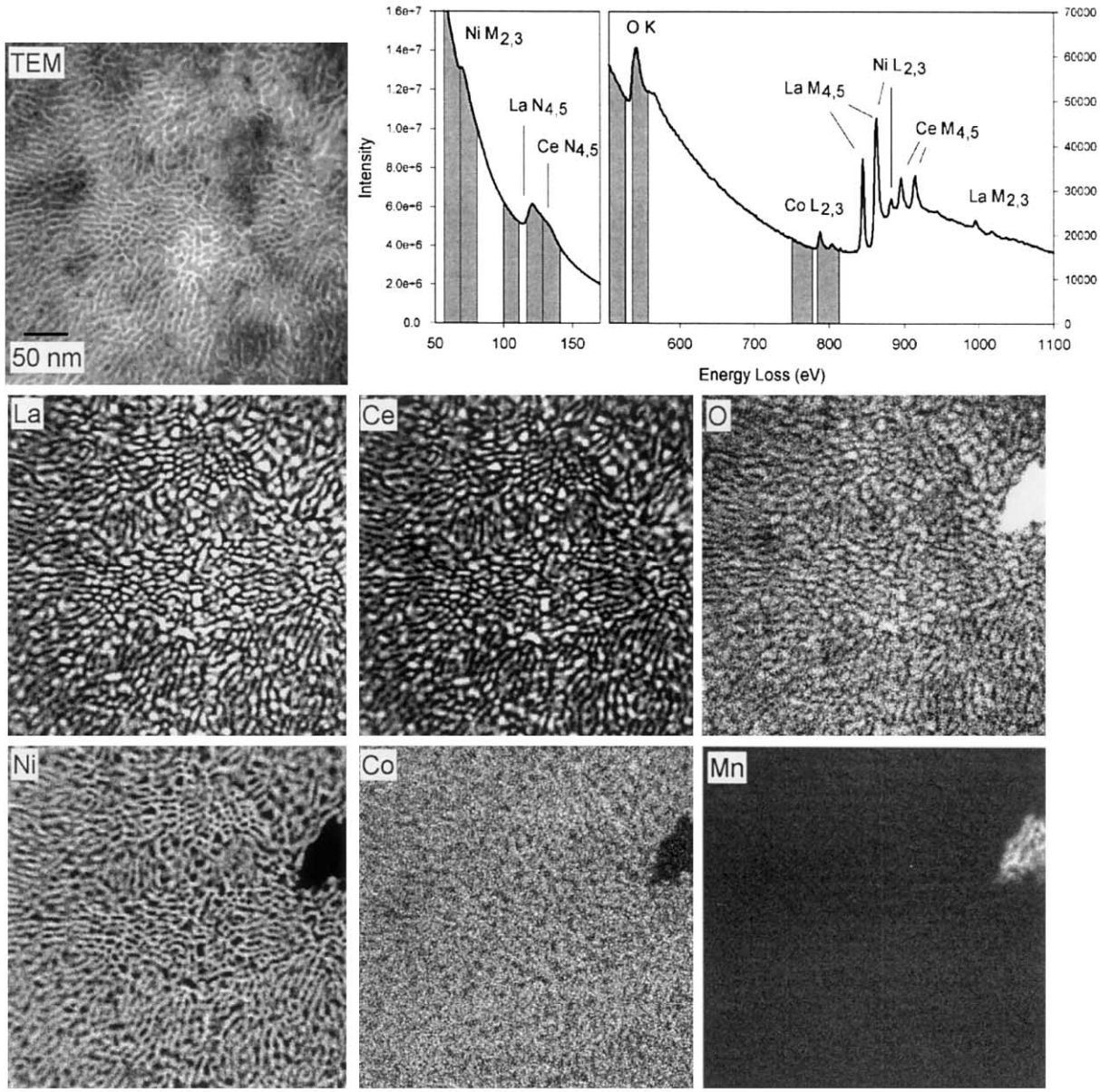

Fig. 4. EFTEM investigation of a rapidly cooled La-based cermet; TEM bright-field image with integral EELS-spectrum recorded from the specimen region shown in the TEM image with the positions of the energy-filtered images; La and Ce $N_{4,5}$ jump ratio images and O K jump ratio image revealing the distribution of La–Ce phase containing also oxygen; d. Ni $M_{2,3}$ and Co $L_{2,3}$ jump ratio images showing the distribution of the Ni–Co phase and Mn $L_{2,3}$ jump ratio image showing a Mn-rich phase.

From the conventional TEM-bright field image given in Fig. 4, the structure of the as-quenched material appears very complicated, which could not be fully characterized by TEM dark-field imaging and electron diffraction until now. Fig. 4 shows a series of jump ratio images acquired by

selecting the different energy-loss signals visible in the EELS-spectrum. In this case recording of elemental maps is very difficult due to severe edge overlap: In the low-loss region the $N_{4,5}$ edges of La and Ce overlap as do the La $M_{4,5}$, the Ni $L_{2,3}$ and the Ce $M_{4,5}$ edges in the high loss region. In contrast to the TEM-image the EFTEM elemental maps show a distinct difference in the intensity distribution which can be clearly attributed to different phases. In the La $N_{4,5}$ and Ce $N_{4,5}$ maps the same specimen areas appear bright which means that these regions correspond to a La and Ce rich phase. Comparison with the O K jump ratio map reveals that this phase contains also oxygen, but it is not clear from the present study, if oxygen is introduced by air cooling of the sample or during TEM specimen preparation (eg via surface oxidation of the thin ion-milled sample). The Ni $M_{2,3}$ map shows the distribution of the Ni-rich phase, but due to the relatively low Co concentration the Co $L_{2,3}$ map does not allow correlation with either the La–Ce-oxide phase or with the Ni rich alloy. This means that Co is less evenly distributed. On the other hand, local enrichments of a manganese-rich phase can be observed in the Mn $L_{2,3}$ elemental map; a comparison of the Mn and O maps shows that these phase is a manganese oxide.

Consequently, EFTEM allows visualization of the distribution of the chemical phases occurring in a rapidly cooled $LaNi_5$ alloy: a La-Ce-(O) compound, an Ni–Co alloy and manganese oxide. The dimensions of the composition modulations range from about 3 to 10 nm and their morphology is quite similar to those found in spinodal decomposition. In order to obtain a more detailed understanding of the decomposition process and to explain the high oxygen concentration, further investigations such as electron diffraction and/or quantitative elemental mapping are necessary.

3.2. Nanoscale Fe–Tb multilayers

The physical properties of multilayer films depend critically on both the microstructure and the chemical profile across the layers, often at a scale close to the atomic level, because of the small thickness of the layers. For instance, magnetic devices employ a multilayer structure with thicknesses of several nanometers. Since their magnetic properties are so sensitive to the thickness and flatness of each layer, elemental mapping of cross-sectioned multilayer specimens is necessary to correlate the properties of these materials with their micro structure. A typical example for such a multilayer exhibiting perpendicular magnetic anisotropy is the system Fe/Tb which is of potential interest for vertical magnetic data storage. This multilayer has been prepared by sputtering thin terbium and iron layers on a silicon single crystal covered by a native oxide film. The thickness of the terbium and iron layers is about 2 and 3 nm, respectively [23]. A cross-section of the multilayer has been carefully aligned so that the interfaces are parallel to the direction of the electron beam. However, the TEM bright field image shown in Fig. 5 does not reveal the morphology and sequence of the individual layers. In order to provide this important information, energy-filtered images have been acquired at the energy-losses shown in Fig. 5 and the elemental maps have been calculated by using the three window method: The Tb $N_{4,5}$ and the Fe $M_{2,3}$ maps show the layer sequence very clearly and even the 2 nm thin terbium layer can be clearly resolved. The multilayer exhibits well defined interfaces and intermixing between the layers or growth defects occur only occasionally. Alternatively, this multilayer stack was also studied by electron diffraction thus yielding a planar pair distribution function which gives information upon atomic distances in the layers and therefore allows determination of the intermixing between the layers [24]. These investigations showed minor intermixing between the layers thus confirming the results of the elemental mapping technique.

Finally, it has to be emphasized that the EFTEM technique is the method of choice for characterizing multilayers, because it allows the characterization of a larger specimen region (which is thus more representative of the real structure) than it would be possible by a single EELS line scan perpendicular to the layers. In a similar way, EFTEM elemental mapping has been useful for studying thick film Ti/Al nanolaminates

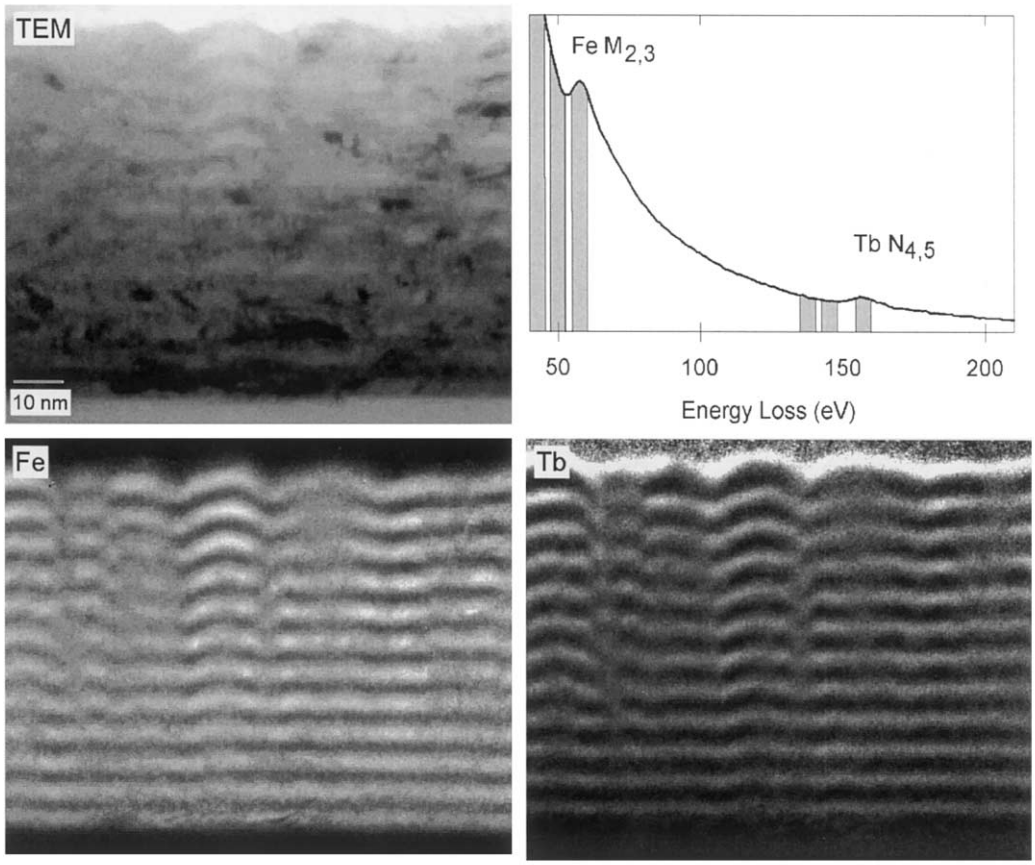

Fig. 5. EFTEM investigation of a multilayer consisting of 2 nm Tb and 3 nm Fe; TEM bright-field image with the EELS-spectrum recorded from the specimen region shown in the TEM image with the positions of the energy-filtered images; Fe elemental map recorded with the Fe $M_{2,3}$ edge and Tb elemental map recorded with the Tb $N_{4,5}$ edge.

consisting of nanoscale multilayers with nominal layer spacings of 3 nm Ti and 8 nm Al, respectively [25].

4. Conclusions

We have demonstrated that EFTEM compositional mapping is a powerful method for characterizing nanostructured materials over large fields of view, offering information which cannot be easily obtained by any other analytical technique.

The main advantages of EELS and EFTEM are: (1) The EELS data can be acquired with nanometer resolution, thus rivalling or exceeding x-ray absorption from a dedicated synchrotron source not only in spatial resolution but sometimes also in spectral quality. (2) EFTEM elemental maps are ideal for mapping high local concentrations distributed over rather large specimen areas. (3) The distribution maps of most elements ranging from Li to U can be acquired in much shorter times than with the complementary scanning techniques.

Acknowledgements

The authors gratefully acknowledge financial support through the ‘Fonds der wissen-

schaftlichen Forschung' (FWF) within the Special Research Program 'Electroactive Materials'. The authors thank Albert Brunegger for the preparation of TEM specimen of the $LaNi_5$ sample.

References

[1] F. Hofer, W. Grogger, P. Warbichler, I. Papst, Microchim. Acta 132 (2000) 273–288.
[2] R.D. Leapman, J.A. Hunt, J. Microsc. Soc. Am. 1 (1995) 93–108.
[3] W. Grogger, F. Hofer, P. Warbichler, G. Kothleitner, Microsc. Microanal. 6 (2000) 161–172.
[4] A.L.D Beckers, W.C. De Bruijn, M.I. Cleton-Soeteman, H.G. Van Eijk, E.S. Gelsema, Micron 28 (1997) 349–360.
[5] J. Mayer, U. Eigenthaler, J.M. Plitzko, F. Dettenwanger, Micron 28 (1997) 361–370.
[6] R.F. Egerton, Electron-Energy Loss Spectroscopy in the Electron Microscope, Plenum, New York, 1996.
[7] L. Reimer, Energy-Filtering Transmission Electron Microscopy, Springer, Berlin, 1995.
[8] H. Shuman, C.-F. Chang, A.P. Somlyo, Ultramicroscopy 19 (1986) 121–134.
[9] O.L. Krivanek, A.J. Gubbens, N. Dellby, C.E. Meyer, Microsc. Microanal. Microstruct. 3 (1992) 187–199.
[10] H. Rose, E. Plies, Optik 40 (1974) 336.
[11] W. Probst, G. Benner, J. Bihr, E. Weimer, Adv. Mater. 5 (1993) 297–300.
[12] W.J. De Ruijter, Micron 26 (1995) 247–276.
[13] A.J. Weickenmeier, W. Nüchter, J. Mayer, Optik 99 (1995) 147–154.
[14] D. Bouchet, N. Brun, D. Imhoff, et al., International Centennial Symposium on the Electron, 1999, pp. 247–257.
[15] F. Hofer, W. Grogger, G. Kothleitner, P. Warbichler, Ultramicroscopy 67 (1997) 83–104.
[16] F. Hofer, P. Warbichler. In: M.M. Disko, C.C. Ahn, B. Fultz (eds.), Transmission Electron Energy-Loss Spectroscopy in Materials Science, Wiley, New York (in press).
[17] F. Hofer, P. Warbichler, W. Grogger, Ultramicroscopy 59 (1995) 15–32.
[18] A. Berger, H. Kohl, Optik 92 (1993) 175–193.
[19] G. Kothleitner, F. Hofer, Micron 29 (1998) 349–357.
[20] N. Bonnet, C. Colliex, C. Mory, M. Tence, Scanning Microscopy 2 (Suppl.) (1988) 351–365.
[21] F. Hofer, P. Warbichler, Ultramicroscopy 63 (1996) 21–26.
[22] H. Kronberger, J. Alloys Compounds 253-254 (1997) 87–89.
[23] W. Attenberger, Diploma Thesis, Universität Regenburg (1997), Regensburg, Germany.
[24] J. Zweck, M. Tewes, H. Hoffmann, J. Phys: Cond. Matter 8 (1996) 649–663.
[25] L. Coast-Smith, R. Brydson, P. Tsakiropoulos, et al., Micron 29 (1998) 17–33.